How short-range adhesion slows down crack closure and contact formation

C. Müller ; M. H. Müser ✉

Check for updates

View Online

Export Citation

How short-range adhesion slows down crack closure and contact formation

C. Müller[1] and M. H. Müser[2,a)]

AFFILIATIONS

[1] INM—Leibniz Institute for New Materials, 66123 Saarbrücken, Germany
[2] Department of Materials Science and Engineering, Saarland University, 66123 Saarbrücken, Germany

Note: This paper is part of the JCP Special Topic on Adhesion and Friction.
[a)]Author to whom correspondence should be addressed: martin.mueser@mx.uni-saarland.de

ABSTRACT

While viscoelastic, adhesive contact rupture of simple indenters is well studied, contact formation has received much less attention. Here, we present simulations of the formation of contact between various power law indenters and an adhesive, viscoelastic foundation. For all investigated indenters, we find that the macroscopic relaxation time τ scales approximately with $1/\rho^{1.8}$, where ρ is the range of adhesion. The prolongation of contact formation with Tabor parameter is rationalized by the increased dissipation that short-range adhesion causes on a moving crack.

I. INTRODUCTION

The modeling of mechanical contacts between elastomers and rigid counterfaces has advanced substantially in the recent past.[1–3] In particular, the comparison between simulated contact configurations and real-laboratory images has reached new levels, mainly thanks to improved capabilities of computing and measuring detailed features in partial contacts of nominally flat surfaces.[1,4–8] However, the progress made pertains mostly to situations where either the experiment is conducted quasi-statically or multi-scale roughness is insignificant. Viscoelastic simulations with roughness on separate length scales remain scarce.[8–10] As a consequence, it remains difficult to ascertain or to predict when contact hysteresis in a given system is mostly viscoelastic in nature[11] or caused by elastic multistability[12–14] and whether their effects are deemed additive[10] or inseparable.[8] When assessing contact hysteresis, it is as important to describe contact formation as contact rupture.[15] However, despite continuous progress in the simulation of viscoelastic, adhesive contacts,[16–20] contact formation is explored rather little although it is similarly important as contact rupture. It could be one reason for the so-called Monday morning problem, which refers to the sticking of valves in production engines after resting over the weekend. Further applications, where (slow) contact formation matters, are hydraulic and pneumatic seals or adhesive gripping devices.

The difficulty of simulating adhesion-driven contact formation involving soft matter is that the short-range nature of adhesion must be accounted for, even for macroscopic objects. First, non-contact puts much greater demands on the range of adhesion than contact:[15,21] While a Tabor parameter $\mu_T \approx 5$ (μ_T is a dimensionless measure inversely proportional to the range of adhesion and introduced in detail further below) suffices to reproduce the $\mu_T \to \infty$ load–displacement curves under retraction, the energy loss would be less than 50% of the real value, due to a premature jump into contact. Unfortunately, short-range adhesion requires a modeler to use small mesh sizes to avoid discretization artifacts, most notably lattice trapping.[15] Making matters worse, the errors in energy hysteresis disappear only with the inverse cube of the linear mesh-element size.[15] Second, short-range adhesion enhances the dissipation of a moving crack or contact line,[22–26] whereby not only crack opening but also crack closure is impeded, which in turn puts large demands on the computing time.

The discussion above implies that simulating effectively viscoelastic processes using relatively coarse scales might be achievable by reinterpreting the time scales used in the viscoelastic model. This would be possible if multiplying the range of adhesion by a factor s accelerated the dynamics by a power of s. Testing for the possibility of such a mapping was the original motivation for the research reported in this work. However, the simulations can also serve as a test for theoretical predictions on contact closure and extend the

number of geometries, for which gap closure is investigated. In this context, our focus is on indenter shapes, where the height of the indenter is a power law of the distance from the indenter's symmetry axis. This problem class offers the greatest potential for us to exploit the similarity of solutions.

The remainder of this work is organized as follows: The methods used are laid out in Sec. II, results are presented in Sec. III, and conclusions are drawn in Sec. IV. Some scaling arguments allowing the Tabor parameter to be generalized to adhesive power law indenters are given in the Appendix.

II. METHODS

We use Green's function molecular dynamics (GFMD),[27] which is a boundary-element method for the simulation of linearly (visco)elastic contact problems assuming elastic bodies to be isotropic in planes normal to their (originally flat) surface and to be periodically repeated in that plane. We focus on normal, frictionless contacts within linear elasticity. Our systems consist of various perfectly rigid indenters and a homogeneous and isotropic, linearly viscoelastic body described in the continuum limit.

The shape of the indenter is given by

$$h(r) = \frac{R}{n}\left(\frac{r}{R}\right)^n, \qquad (1)$$

where R has the unit of length and corresponds to a radius of curvature for a Hertzian ($n = 2$) indenter, while r is the distance from the indenter's symmetry axis. For a conical indenter ($n = 1$), $h(r)$ could be written as $h(r) = r \tan \varphi$, in order to implement different opening angles φ. Investigated exponents are $n = 1$ for a conical indenter, $n = 2$ for a Hertzian indenter, and $n = 3$ as well as $n = 4$ as crude approximations for a flat punch. A true flat punch has no interesting contact formation dynamics, as its instantaneous contact radius is identical to the relaxed one.

Indenter and elastic body interact through a cohesive-zone model that is twice differentiable everywhere but in one isolated point, which proves to be useful for numerical or stability reasons.[15] It is given by an interaction potential density of

$$V_{int}(g) = -\gamma \times \begin{cases} 0 & \text{if } \rho \le g, \\ \{1 + \cos(\pi g/\rho)\}/2 & \text{if } 0 < g < \rho, \\ \{1 - (\pi g/2\rho)^2\} & \text{else.} \end{cases} \qquad (2)$$

Here, g refers to the gap or interfacial displacement between elastomer and indenter, γ is the energy gained per unit area when indenter and elastomer touch, while ρ is the range of adhesion. In all investigated systems, a numerical value of $\gamma = 0.01 \, E^* R$ is assigned. The numerical value of ρ was adjusted according to the individual Tabor parameters. In principle, ρ could be set to a smaller value for negative than for positive gaps to better mimic hard-wall repulsion. However, since all reported simulations addressed rather short-ranged adhesion and thus small ρ, we used the same value for ρ for attraction and repulsion.

The elastic energy of a relaxed body (under an external surface stress) is given by

$$V_{ela} = \sum_{\mathbf{q}} \frac{q E^*}{4} |\tilde{u}(\mathbf{q})|^2, \qquad (3)$$

where $\mathbf{q}$ is an in-plane wave vector, or wave number for one-dimensional interfaces, q is its magnitude, while E^* is the static contact modulus and $\tilde{u}(\mathbf{q})$ the Fourier transform of the displacement field. However, as we study a viscoelastic system, E^* is made frequency dependent. Our default model consists of a single Maxwell element in parallel with a spring, yielding a frequency-dependent contact modulus of

$$E^*(\omega) = E_0 \frac{1 + s\omega^2 \tau_{Mxw}^2 + i(s-1)\omega\tau_{Mxw}}{1 + \omega^2 \tau_{Mxw}^2} \qquad (4)$$

with $s \equiv E_\infty^*/E_0^* = 100$, where E_0^* and E_∞^* are the quasi-static and the high-frequency elastic moduli, respectively. The model is implemented as described in Ref. 8. E_0^* is used as the unit for pressure, while times are reported in units of τ_{Mxw}, unless stated otherwise. Any deviation from our default model is explicitly pointed out. For example, in one case, the surface modes are coupled to three rather than to one Maxwell element. The real and imaginary parts of $E^*(\omega)$ are shown in Fig. 1 for the three-element model and the default, one-element model. The "weights" $E_0^{(n)}$ and relaxation times $\tau_{Mxw}^{(n)}$ in the three-element models are chosen as $E_0^{n+1} = 6E_0^n$ and $\tau_{Mxw}^{(n+1)} = \tau_{Mxw}^{(n)}/6$.

While a "brute-force" Fourier method is certainly not the most effective approach to address the questions in this paper, it
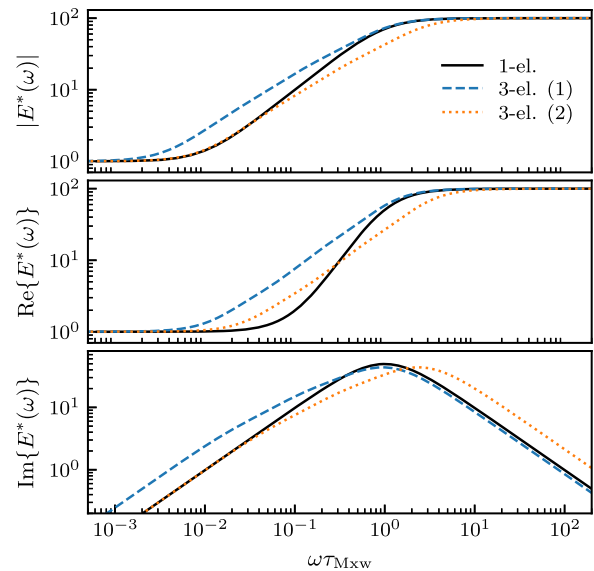
FIG. 1. Absolute value $|E^{*\prime}(\omega)|$ (top), real part $E^{*\prime}(\omega)$ (middle), and imaginary part $E^{*\prime\prime}(\omega)$ (bottom) of the contact modulus for a one-element (1-el, solid lines), standard linear-solid model and a three-element (3-el, dashed and dotted lines) model. The frequency is expressed in inverse units of τ_{Mxw} of the one-element model (blue line), while the data for the three-element are shifted one time to have a similar high-frequency (dashed, blue line) and one time to have a similar low-frequency (dotted, orange line) modulus as the one-element model.

is sufficiently efficient to obtain satisfying answers. Moreover, by addressing primarily line contacts having a formal interfacial dimension of $D = 1$, much of the computational overhead spent on not exploiting the symmetry of the problem in $D = 2$ is alleviated.

The most critical dimensionless parameter for a (force-free) adhesive contact of a Hertzian indenter is the Tabor parameter μ_T. It is inversely proportional to the range of adhesion and is designed such that $\mu_T \gg 1$ makes a (quasi-static) contact behave as in the limit for zero-range adhesion, which was first solved analytically by Johnson, Kendall, and Roberts (JKR)[28] for $n = 2$ and $D = 2$. For arbitrary n at $D = 2$, the contact problem can be solved using Sneddon's method.[29,30] Less relevant for most real purposes, but easier to tackle numerically and theoretically, is long-range adhesion. For $D = n$, adhesion effectively acts like an external load that does not depend on ρ for $\rho \to \infty$ or $\mu_T \to 0$ when γ and R are fixed, as is readily seen using the Bradley model,[31] which becomes exact in the long-range limit. Its analysis also reveals that a physically meaningful long-range-adhesion limit does not exist for $n \neq D$, because the offset load vanishes ($n > D$) or diverges ($n < D$) for a diverging ρ at fixed γ and R.

Zheng and Yu[32] generalized the Tabor parameter for arbitrary power law indenters to

$$\mu_T = \frac{R}{\rho}\left(\frac{\gamma}{RE^*}\right)^{n/(2n-1)}. \tag{5}$$

after solving the contact mechanics of adhesive power law indenters in the Dugdale approximation. In the Appendix, we identify the same expression using rather simple, dimensional analysis, which is also valid for an interfacial dimension of $D = 1$. In the following, we will usually report μ_T rather than the range of adhesion ρ. Note that the precise value for μ_T would differ if the ratio γ/σ_{max} were used instead of ρ in Eq. (5).

In this work, we study exclusively crack closure dynamics under zero external load. We focus on the time evolution of the contact radius $r_c(t)$, which we define to be the distance from the indenter's symmetry axis to the point where the tensile stress takes its maximum, specifically, the distance in a direction parallel to a main axis of the simulation cell rather than its diagonal, though the two measures are very close to each other and thus show identical scaling. A small relaxation run is done first, using "regular" rather than viscoelastic GFMD, during which the elastomer is allowed to relax to the shape that it would have under the assumption that E_∞^* rather than E_0^* was its static contact modulus. The estimates of quasi-static contact properties are obtained from similar calculations with the proper static contact modulus E_0^*. This way, initial contact radii $r_{in} \equiv r_c(t = 0)$ and quasi-static contact radii $r_{qs} \equiv r_c(t \to \infty)$ can be determined with high accuracy. Results for $r_c(t)$ are reported in terms of a relaxation function defined as

$$C(t) \equiv \frac{r_c(t) - r_{in}}{r_{qs} - r_{in}}. \tag{6}$$

While we do not yet have experimental reference data, it might be important to stress that it might be difficult to rigorously define r_{in} in real experiments, since contact with a rigid counter body cannot be simply switched on as in a computer simulation, while inertial effects would prevent an immediate contact at $t = 0^+$ with the high-frequency modulus from occurring. Thus, we expect deviations

between our idealized model and real experiments in the very early stages of contact formation to be unavoidable.

III. RESULTS

While this study focuses on contact formation for different tip geometries, we first wish to analyze how details of the viscoelastic model affect the dynamics. To this end, Fig. 2 contrasts the gap closure for the one-element model and the three-element model introduced in Sec. II. Both rheological models reveal the same generic features of the crack closure process for power law indenters: Early-time dynamics, in the specific example for $t \lesssim 10\tau_{Mxw}$, a regime where the contact radius depends approximately logarithmically on time, i.e., for times $10 \lesssim t/\tau_{Mxw} \lesssim 10^4$, and a final regime at $t \gtrsim 10^4\tau_{Mxw}$, which has an exponential time dependence according to

$$C(t \to \infty) - C(t) \propto \exp(-t/\tau), \tag{7}$$

which defines the macroscopic or largest relaxation time τ. While the relaxation in the intermediate time curve is somewhat flattened for the three-element model compared to the one-element model, the contrast in different $r_c(t)$ curves in Fig. 2 appears somewhat less noticeable to the eye than those of the frequency-dependence of the elastic modulus shown in Fig. 1. Interestingly, though perhaps not surprisingly, the early-time (later-time) dynamics of the two models superimpose reasonably well when the relaxation times of the three-element model are scaled such that the high-frequency (low-frequency) $E''(\omega)$ or $|E(\omega)|$ exhibits similar behavior. In the following, we will merely consider the one-element model, widely known also as the standard linear solid (SLS).

Similar crack closure dynamics as those just discussed are maintained when extending the range of Tabor parameters. To this end, $C(t)$ rather than $r_c(t)/R$ is shown for different μ_T, one time for two-dimensional interfaces in Fig. 3 and one time, as before, for one-dimensional interfaces in Fig. 4. Similar behavior is revealed in both figures. A double logarithmic representation was chosen for them
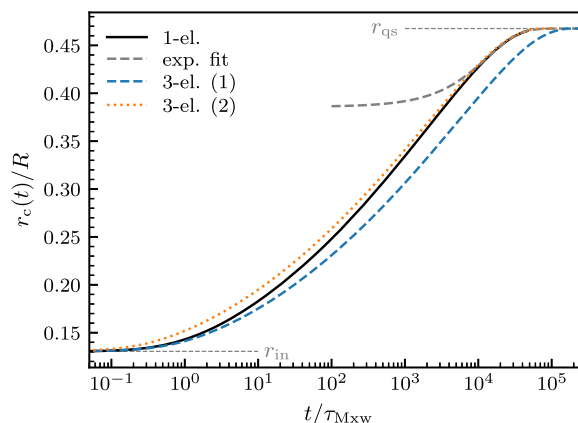

FIG. 2. Contact formation of the one-element model and the three-element model(s), whose frequency-dependent elastic modulus is shown in Fig. 1; $D = 1$, $n = 2$, $\mu_T = 7.2$. Thin gray lines indicate the instantaneous contact radius for $t \to 0$ as well as the final exponential approach (exp) to the quasi-static value r_{qs} reached at $t \to \infty$.
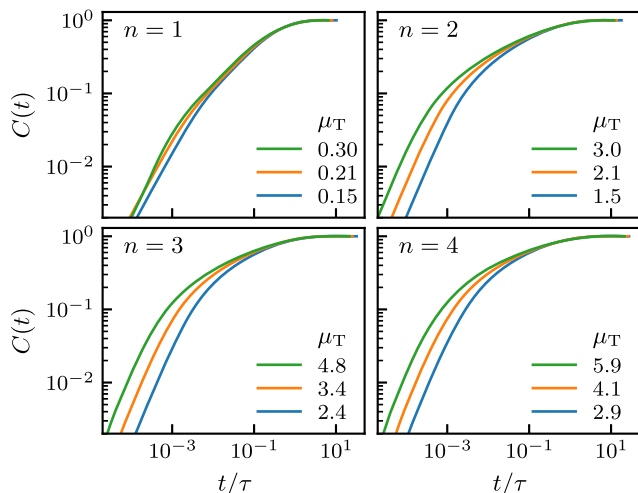
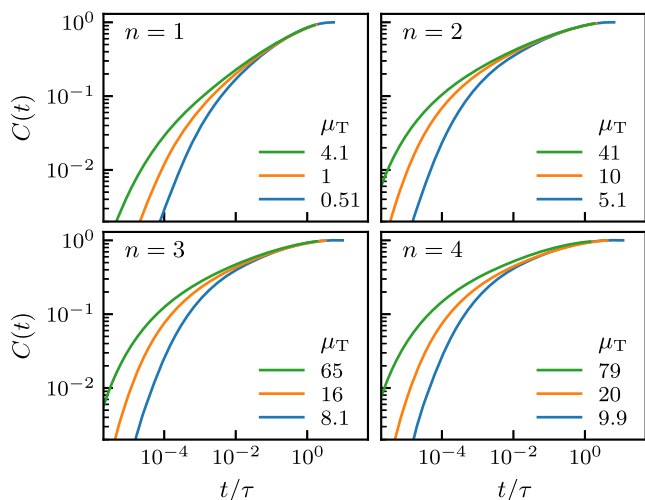**FIG. 3.** Crack closure dynamics for different axisymmetric tips.

FIG. 4. Crack closure dynamics for different one-dimensional tips.

as to highlight differences in the functional form of $C(t)$ during the early-time dynamics. Note that the time is expressed in units of τ, which allows us to reveal that $C(t/\tau)$ is quite insensitive to μ_T at sufficiently large t. The collapse of curves when represented as $C(t/\tau)$ improves with increasingly large μ_T. Factors and related information helpful to reconstruct the full $r_c(t/\tau)$ are collected in Table I, however, each time only for the largest Tabor parameter.

The increase in relaxation time compared to the times associated with the Maxwell element can certainly be related to the increased dissipation that short-range adhesion causes in a propagating crack.[22,24,25] Initial dynamics are relatively fast, when the crack-tip radius is large and thus dissipation small[10,26] but then slows down as the crack-tip radius becomes smaller, while the slopes of the displacement field increase. For the investigated tip shapes, we find the relaxation times to scale approximately with $\mu_T^{1.8}$. This is true

TABLE I. Quantities needed to reconstruct the full $r_c(t)$ dependence, for each investigated geometry at the largest investigated Tabor parameter μ_T. Radii are given in units of the (generalized) radius of curvature R and times in units of τ_{Mxw}. $\tau_{1/2}$ is defined implicitly by $C(\tau_{1/2}) = 1/2$.

D	n	r_{in}	r_{qs}	$\tau_{1/2}$	τ	μ_T	s
1	1	0.0021	0.062	130	1060	4.1	19
	2	0.11	0.46	23	910	41	5.9
	3	0.28	0.67	9.8	670	65	4.1
	4	0.41	0.78	6.6	750	79	3.5
2	1	0.013	0.10	23	110	0.30	24
	2	0.17	0.52	3.7	83	3.0	7.2
	3	0.35	0.71	1.6	45	4.8	4.9
	4	0.48	0.81	1.0	36	5.8	4.2

for the ultimate relaxation time τ as well as intermediate relaxation times τ_x defined by $C(\tau_x) = x$ with $x \gtrsim 0.5$. To make the different data sets appear in a rather narrow range, the Tabor parameter was scaled (multiplied) with a scaling variable s, while the relaxation time was divided by $s^{1.8}$ (Fig. 5).

It remains to be discussed to what degree our results depend on the precise form of the cohesive-zone model (CZM). To address this issue, we repeated some simulations using a Dugdale model[33] and found the same $\tau \propto \mu_T^{1.8}$ scaling law as when using Eq. (2). Prefactors of the scaling laws cannot be compared directly because the length scale used in the definition of the Tabor parameter can be either the literal range of adhesion ρ or the ratio of surface energy and maximum tensile stress. Taking the geometric mean of those two options makes the Dugdale potential relax roughly 15% more slowly than the default CZM with the same Tabor parameter. We attribute the slight increase in relaxation time and thus dissipation by the Dugdale model to the discontinuity of the CZM at the cutoff. It leads to
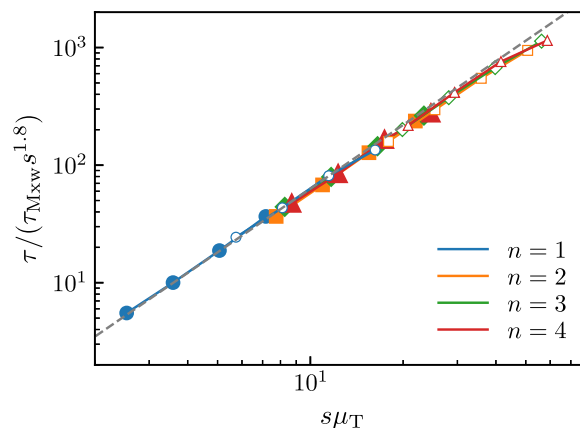

FIG. 5. Scaled relaxation time as a function of a scaled Tabor parameter for different power law indenters and interfacial dimensions. Open and filled symbols refer to $D = 1$ and $D = 2$, respectively. Moreover, $n = 1$ (blue circles), $n = 2$ (orange squares), $n = 3$ (green diamonds), and $n = 4$ (red triangles). The dashed, gray line shows the power law $(s\mu_T)^{1.8}$.

a diverging second derivative, which in turn induces enhanced local surface velocity for a moving crack and thus enhanced velocity gradients in the material and increased total dissipation compared to more smoothly evolving CZMs.

IV. CONCLUSIONS

In this work, we confirmed numerically that the crack closure dynamics of indenters with power law profile in contact with an adhesive, linearly viscoelastic foundation has a universal behavior, at least at the late stages of the contact formation process when the contact radius has grown to a size that adhesion can be labeled short-ranged. Analysis of the final stages of the contact formation reveals that the relaxation times increase approximately with the inverse range of adhesion to the power of 1.8. Since Tabor parameters can be quite large in practical applications, this means that crack closure can last rather long times. To give an admittedly extreme example, assuming $E^* = 10$ MPa, $\gamma = 40$ mJ/m^2, $R = 20$ μm, and a range of adhesion typical for Lennard-Jones interactions, say $\rho = 3.5$ Å, yields $\mu_T = 195$. Thus, using the data for $D = n = 2$ in Table I, we obtain $\tau/\tau_{\text{Mxw}} \approx 83 \cdot (195/3)^{1.8} \approx 0.15 \cdot 10^6$. Making the link to real viscoelastic materials is challenging, because they have a broad distribution of relaxation times, which are quite sensitive to temperature and materials composition. This in turn makes it difficult if not impossible to state a generally valid numerical value for τ_{Mxw}. However, if a dynamical analysis is known, an upper estimate for τ_{Mxw} should be given by the equation $E''(1/\tau_{\text{Mxw}}) = E_0$ on the small-frequency branch of the loss modulus.

Unfortunately, it is not clear to what degree the scaling might be affected by small-scale roughness. In the extreme case, there will be contact line pinning due to elastic multistability, which can be caused by structural heterogeneity.[14] In this case, our estimates would only imply a crude lower bound for the contact formation time. A hint in this direction comes from previous simulations.[8] They mimicked successfully dynamical experiments on the adhesion between an elastomer and a flat punch to which (single-sinusoidal) small-scale roughness was added. In that work, we had identified a steeper dependence of relaxation times on the range of adhesion than in the present work, although our old estimate was based on an analysis, which was much less systematic than the one presented here.

AUTHOR DECLARATIONS

Conflict of Interest

The authors have no conflicts to disclose.

Author Contributions

C. Müller: Conceptualization (equal); Data curation (lead); Formal analysis (equal); Investigation (lead); Methodology (equal); Software (lead); Writing – original draft (supporting); Writing – review & editing (equal). **M. H. Müser**: Conceptualization (equal); Formal analysis (equal); Methodology (equal); Supervision (lead); Writing – original draft (lead); Writing – review & editing (equal).

DATA AVAILABILITY

The data that support the findings of this study are available from the corresponding author upon reasonable request.

APPENDIX: SCALING ANALYSIS AND GENERALIZED TABOR PARAMETER

While the contact mechanics of both short-range[30] and finite-range[32] adhesive power law indenters have been solved, it might be beneficial to have simple arguments allowing one to estimate pull-off forces, work of adhesion, and Tabor parameters in simple terms up to prefactors of order unity without having to embark on the high level of complexity pioneered by Maugis.[34] For this purpose, it is helpful to realize that the crack closure dynamics for a given $E(\omega)$ can only depend on the dimensionless numbers describing the problem, i.e., n and μ_T. In the following, we derive an expression, which, up to constants of order unity, gives the generalized Tabor parameter. To this end, we define μ_T such that $\mu_T \equiv 1$, when simple estimates for the stress-standard deviation in the limit of short-range adhesion match the maximum tension for finite-range adhesion. Our treatment also allows us to identify scaling relations for power law indenters. While similar relations can be deduced from existing literature, we believe our derivation to be original while requiring close to the least possible amount of prior background on contact mechanics and graphite, chalk, ink, or toner in order to arrive at generally valid scaling relations.

For a given shape (shp) of the displacement field, be it the zero-load (zl) or the pull-off (po) shape, the elastic energy U_{el} in areal contacts ($D = 2$) or its line density $u_{\text{el}} \equiv \Delta U_{\text{el}}/\Delta L_y$ in line contacts ($D = 1$) can only be of the form

$$U_{\text{el}} = g^{\text{shp}}_{n,2} E^* a h^2(a) \quad \text{for } D = 2, \tag{A1a}$$

$$u_{\text{el}} = g^{\text{shp}}_{n,1} E^* h^2(a) \quad \text{for } D = 1, \tag{A1b}$$

in the limit of short-range adhesion. Here, a is the contact radius, while the $g^{\text{shp}}_{n,D}$ are constants that depend on the exponent n, the interfacial dimension D, and on the shape of the displacement field. The corresponding total surface energy U_s or line density u_s gained on making contact are

$$U_s = -\pi a^2 \gamma \quad \text{for } D = 2, \tag{A2a}$$

$$u_s = -2a\gamma \quad \text{for } D = 1. \tag{A2b}$$

Eliminating $h(a)$ with the help of Eq. (1) and minimizing the total energy in the load-free case w.r.t. a yield a zero-load radii of

$$\frac{a_{\text{zl}}}{R} = {}^{2n-1}\!\!\sqrt{\frac{c\gamma}{E^* R}} \quad \text{with } c = \begin{cases} \dfrac{2\pi n^2}{(2n+1)g^{\text{zl}}_{n,2}} & \text{for } D = 2, \\[2ex] n/g^{\text{zl}}_{n,1} & \text{for } D = 1. \end{cases} \tag{A3}$$

For the surface of a semi-infinite solid, the stress variance is nothing but $\Delta\sigma^2 = (E^*/2)^2 \langle(\nabla u)^2\rangle$, where $\langle\cdots\rangle$ denotes spatial average. This relation is heavily exploited in Persson's contact mechanics theory for the contact mechanics of randomly rough contacts. However, it also turns out useful for deterministic tip shapes,

in particular power law indenters, when restricting the spatial average over the true contact. Since the mean-square height gradient $\bar{g}_c^2$ averaged over the contact satisfies

$$\bar{g}_c^2 = \left\langle (\nabla u)^2 \right\rangle_c$$
$$= \left(\frac{a}{R} \right)^{2n-2} \times \begin{cases} 1/n & \text{for } D = 2, \\ \dfrac{1}{2n-1} & \text{for } D = 1, \end{cases} \quad \text{(A4)}$$

the stress variance in the limit of short-range adhesion is roughly on par with the square of the maximum tension if

$$E^* \left(\frac{\gamma}{E^* R} \right)^{(n-1)/(2n-1)} = \frac{\gamma}{\rho}, \quad \text{(A5)}$$

where we suppressed all numerical prefactors, which are deemed to be usually of order unity. We define the Tabor parameter to be unity for the range of adhesion satisfying Eq. (A5) so that

$$\mu_T = \frac{\gamma}{E^* \rho} \left(\frac{\gamma}{E^* R} \right)^{(1-n)/(2n-1)}, \quad \text{(A6)}$$

which is identical to Eq. (5).

As a side comment, we note that our scaling analysis also allows the pull-off force F_{po} and the work of adhesion W_{po} in $D = 2$ and their corresponding line densities using lower-case letters in $D = 1$ to be estimated. To this end, we assume that the mean contact stress at pull-off scales linearly with the stress-standard deviation at zero load. Thus, $F_{po} \propto a_0^2 E^* \bar{g}_c$ for $D = 2$ while $f_{po} \propto a_0 E^* \bar{g}_c$ for $D = 1$ so that

$$F_{po} \propto E^* R^2 \left(\frac{\gamma}{E^* R} \right)^{(n+1)/(2n-1)} \quad \text{for } D = 2, \quad \text{(A7a)}$$

$$f_{po} \propto E^* R \left(\frac{\gamma}{E^* R} \right)^{n/(2n-1)} \quad \text{for } D = 1, \quad \text{(A7b)}$$

which satisfies well-known relations like $F_{po} \propto \gamma R$ for a regular Hertzian geometry ($n = 2, D = 2$) or $F_{po} \propto \sqrt{E^* \gamma R^3}$ for a regular flat punch ($n \to \infty, D = 2$). The work of adhesion of a power law indenter can only scale as the product of surface energy and (zero-load) contact area so that

$$W_{po} \propto \gamma R^2 \left(\frac{\gamma}{E^* R} \right)^{2/(2n-1)} \quad \text{for } D = 2, \quad \text{(A8a)}$$

$$w_{po} \propto \gamma R \left(\frac{\gamma}{E^* R} \right)^{1/(2n-1)} \quad \text{for } D = 1. \quad \text{(A8b)}$$

Thus, the work of adhesion for a flat punch in $D = 1$ and $D = 2$ alike is the same when conducted very slowly or very quickly, i.e., when probing it with the high- or the low-frequency modulus, but it would be large at intermediate pull-off velocities, as argued, for example, in Ref. 26.

REFERENCES

[1] M. H. Müser, W. B. Dapp, R. Bugnicourt, P. Sainsot, N. Lesaffre, T. A. Lubrecht, B. N. J. Persson, K. Harris, A. Bennett, K. Schulze, S. Rohde, P. Ifju, W. G. Sawyer, T. Angelini, H. Ashtari Esfahani, M. Kadkhodaei, S. Akbarzadeh, J.-J. Wu, G. Vorlaufer, A. Vernes, S. Solhjoo, A. I. Vakis, R. L. Jackson, Y. Xu, J. Streator, A. Rostami, D. Dini, S. Medina, G. Carbone, F. Bottiglione, L. Afferrante, J. Monti, L. Pastewka, M. O. Robbins, and J. A. Greenwood, "Meeting the contact-mechanics challenge," Tribol. Lett. **65**, 118 (2017).

[2] D. Wang, G. de Boer, A. Neville, and A. Ghanbarzadeh, "A review on modelling of viscoelastic contact problems," Lubricants **10**, 358 (2022).

[3] M. H. Müser and L. Nicola, "Modeling the surface topography dependence of friction, adhesion, and contact compliance," MRS Bull. **47**, 1221–1228 (2022).

[4] A. I. Bennett, K. L. Harris, K. D. Schulze, J. M. Urueña, A. J. McGhee, A. A. Pitenis, M. H. Müser, T. E. Angelini, and W. G. Sawyer, "Contact measurements of randomly rough surfaces," Tribol. Lett. **65**, 134 (2017).

[5] B. Weber, T. Suhina, T. Junge, L. Pastewka, A. M. Brouwer, and D. Bonn, "Molecular probes reveal deviations from amontons' law in multi-asperity frictional contacts," Nat. Commun. **9**, 888 (2018).

[6] F. Zhang, J. Liu, X. Ding, and R. Wang, "Experimental and finite element analyses of contact behaviors between non-transparent rough surfaces," J. Mech. Phys. Solids **126**, 87–100 (2019).

[7] G. Violano, A. Chateauminois, and L. Afferrante, "Rate-dependent adhesion of viscoelastic contacts. Part II: Numerical model and hysteresis dissipation," Mech. Mater. **158**, 103884 (2021).

[8] C. Müller, M. Samri, R. Hensel, E. Arzt, and M. H. Müser, "Revealing the coaction of viscous and multistability hysteresis in an adhesive, nominally flat punch: A combined numerical and experimental study," J. Mech. Phys. Solids **174**, 105260 (2023).

[9] C. Putignano and G. Carbone, "On the role of roughness in the indentation of viscoelastic solids," Tribol. Lett. **70**, 117 (2022).

[10] F. Pérez-Ràfols, J. S. Van Dokkum, and L. Nicola, "On the interplay between roughness and viscoelasticity in adhesive hysteresis," J. Mech. Phys. Solids **170**, 105079 (2023).

[11] B. Persson, "Contact mechanics for randomly rough surfaces," Surf. Sci. Rep. **61**, 201–227 (2006).

[12] S. Dalvi, A. Gujrati, S. R. Khanal, L. Pastewka, A. Dhinojwala, and T. D. B. Jacobs, "Linking energy loss in soft adhesion to surface roughness," Proc. Natl. Acad. Sci. U. S. A. **116**, 25484–25490 (2019).

[13] V. L. Popov, Q. Li, I. A. Lyashenko, and R. Pohrt, "Adhesion and friction in hard and soft contacts: Theory and experiment," Friction **9**, 1688–1706 (2021).

[14] A. Sanner and L. Pastewka, "Crack-front model for adhesion of soft elastic spheres with chemical heterogeneity," J. Mech. Phys. Solids **160**, 104781 (2022).

[15] A. Wang, Y. Zhou, and M. H. Müser, "Modeling adhesive hysteresis," Lubricants **9**, 17 (2021).

[16] M. Scaraggi and B. Persson, "Theory of viscoelastic lubrication," Tribol. Int. **72**, 118–130 (2014).

[17] M. Scaraggi and B. N. J. Persson, "Friction and universal contact area law for randomly rough viscoelastic contacts," J. Phys.: Condens. Matter **27**, 105102 (2015).

[18] J. S. van Dokkum and L. Nicola, "Green's function molecular dynamics including viscoelasticity," Modell. Simul. Mater. Sci. Eng. **27**, 075006 (2019).

[19] J. S. Van Dokkum, F. Pérez-Ràfols, L. Dorogin, and L. Nicola, "On the retraction of an adhesive cylindrical indenter from a viscoelastic substrate," Tribol. Int. **164**, 107234 (2021).

[20] L. Afferrante and G. Violano, "The adhesion of viscoelastic bodies with slightly wave surfaces," Tribol. Int. **174**, 107726 (2022).

[21] M. Ciavarella, J. Greenwood, and J. Barber, "Effect of tabor parameter on hysteresis losses during adhesive contact," J. Mech. Phys. Solids **98**, 236–244 (2017).

[22] R. A. Schapery, "A theory of crack initiation and growth in viscoelastic media," Int. J. Fract. **11**, 141–159 (1975).

[23] R. A. Schapery, "A theory of crack initiation and growth in viscoelastic media ii. approximate methods of analysis," Int. J. Fract. **11**, 369–388 (1975).

[24] P. G. de Gennes, "Soft adhesives," Langmuir **12**, 4497–4500 (1996).

[25]B. N. J. Persson and E. A. Brener, "Crack propagation in viscoelastic solids," Phys. Rev. E **71**, 036123 (2005).

[26]M. H. Müser and B. N. J. Persson, "Crack and pull-off dynamics of adhesive, viscoelastic solids," Europhys. Lett. **137**, 36004 (2022).

[27]C. Campañá and M. H. Müser, "Practical green's function approach to the simulation of elastic semi-infinite solids," Phys. Rev. B **74**, 075420 (2006).

[28]K. L. Johnson, K. Kendall, and A. D. Roberts, "Surface energy and the contact of elastic solids," Proc. R. Soc. A **324**, 301–313 (1971).

[29]I. N. Sneddon, "The relation between load and penetration in the axisymmetric Boussinesq problem for a punch of arbitrary profile," Int. J. Eng. Sci. **3**, 47–57 (1965).

[30]H. Yao and H. Gao, "Optimal shapes for adhesive binding between two elastic bodies," J. Colloid Interface Sci. **298**, 564–572 (2006).

[31]R. Bradley, "LXXIX. The cohesive force between solid surfaces and the surface energy of solids," London, Edinburgh Dublin Philos. Mag. J. Sci. **13**, 853–862 (1932).

[32]Z. Zheng and J. Yu, "Using the Dugdale approximation to match a specific interaction in the adhesive contact of elastic objects," J. Colloid Interface Sci. **310**, 27–34 (2007).

[33]D. Dugdale, "Yielding of steel sheets containing slits," J. Mech. Phys. Solids **8**, 100–104 (1960).

[34]D. Maugis, "Adhesion of spheres: The JKR-DMT transition using a Dugdale model," J. Colloid Interface Sci. **150**, 243–269 (1992).

22 October 2024 06:01:05